Experiences gained in mapping mire vegetation and topography using airborne discrete-return and waveform-recording lidar and multi-view image analyses

Korpela, I., Koskinen, M., Vasander, H., Holopainen, M. & Minkkinen, K., 2009. Airborne small-footprint discrete-return LiDAR data in the assessment of boreal mire surface patterns, vegetation and habitats. Forest Ecology and Management 258 (7):1549-1566.
http://dx.doi.org/10.1016/j.foreco.2009.07.007

Korpela, I., Haapanen, R., Korrensalo, A., Tuittila, E-S, & Vesala, T. 2019. Vegetation microforms on boreal bogs – fine-scale mapping with airborne waveform-recording LiDAR data and directional signals in aerial images. To appear some day in Mires and Peat.

Ilkka Korpela, U Helsinki (& UEF), Forest Sciences
ilkka.korpela@helsinki.fi
+358-400-218305

Remote sensing workshop, Oulu Sept 23-25, 2019

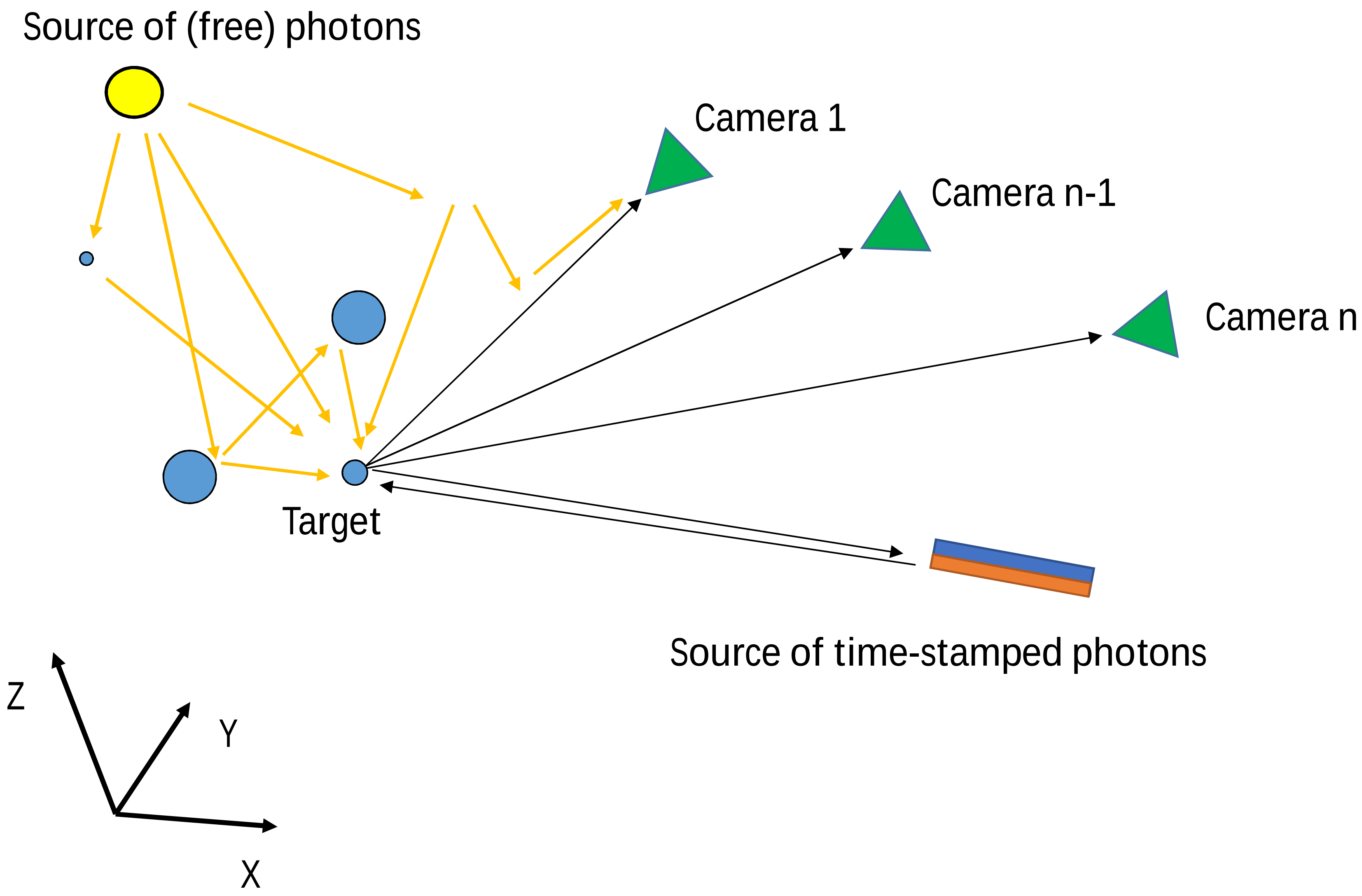

Source of (free) photons
Camera 1
Camera n-1
Camera n
Target
Source of time-stamped photons
Z
Y
X

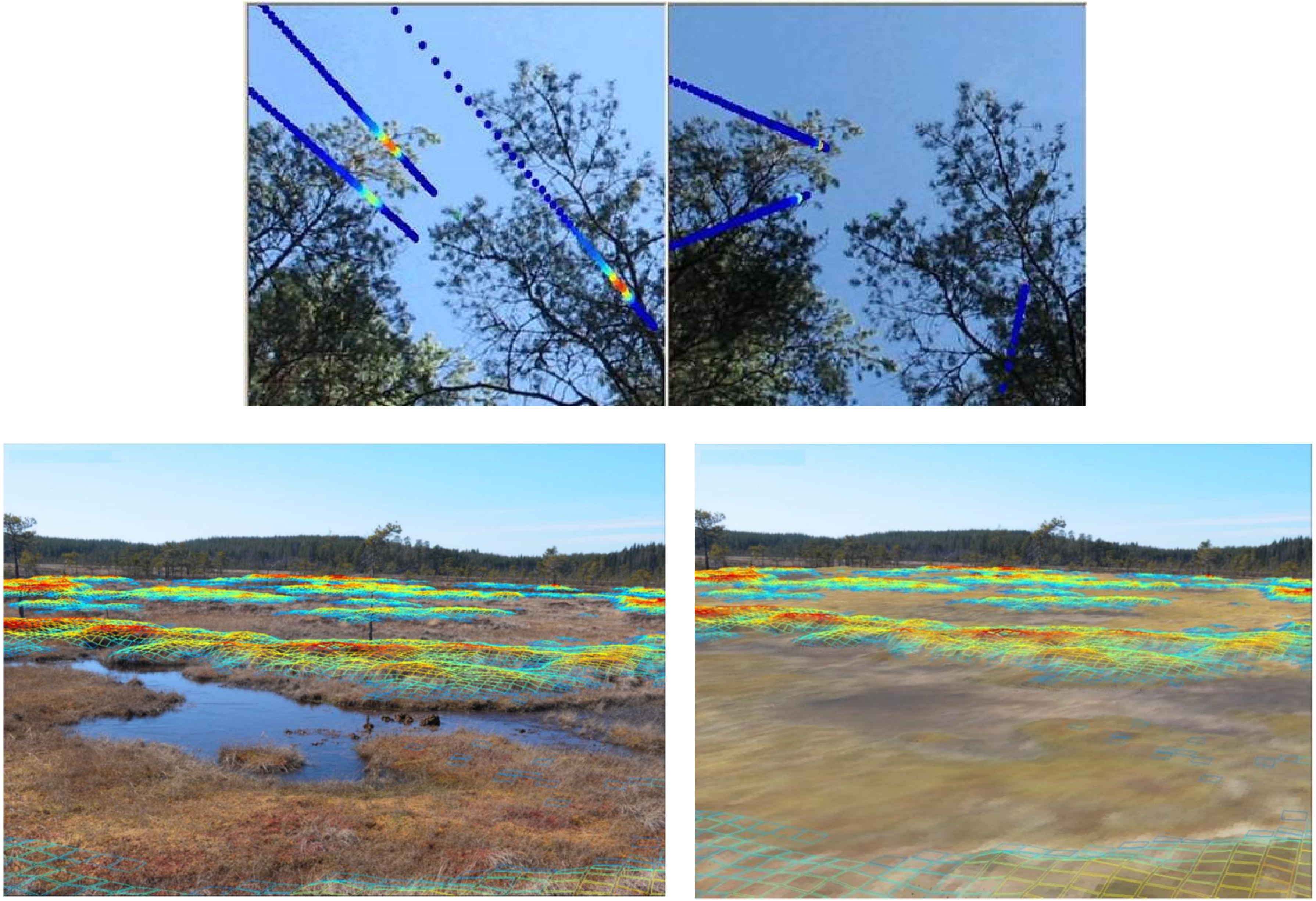

Sensor fusion in 3D is doable nowadays through careful experimentation.

Theses regarding optical RS (of forested – open mires)

GENERAL

- Foliage is dark in VIS, bright in NIR, highly spectrally correlated

- Anything wet or moist is darker

- Optical signals comprise volumetric scattering

- At-target Illumination is a complex issue, At-sensor signal even more

- Usually a strong target effect (variance component)

- Intra-class variation and between-class overlap of spectral features

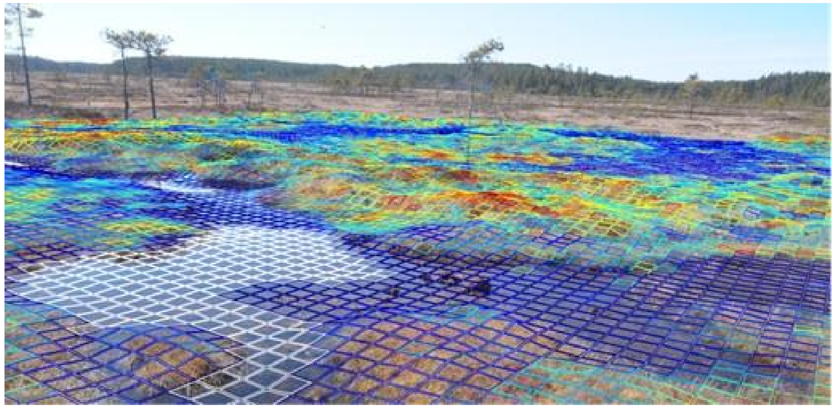

PASSIVE WITH IMAGES

- Reflectance calibration for reliable HCRF observables is at max 10-20% accurate, modern photogrammetric sensors come with absolute calibration (wide band spectral radiance)

- Directional reflectance ('BRDF') effects due to shadow casting are observable but not really exploitable (in a multi-view setup)

- Having hyperspectral observations usually results in compromises regarding sensor geometry

. Otherwise the use of line-sensors would be preferable (BRDF complexity reduction 4D -> 3D)

- Multi-view analyses have become the standard, even multi-image matching (SfM)

- Occlusions and shadow-casting hamper the interpretation as does the contribution from the background (consider e.g. sparse canopies)

- New possibilities for small areas (research, sampling based approach) with unmanned platforms

LIDAR

- LiDAR monostatic view-illumination geometry is superb (4D BRDF -> 2D)

- Pulsed LiDAR enable depth imaging, shorter pulses, stored WFs for better deconvolution

- Receivers are still rather slow (impulse response) and SNR remains low because of eye-safety. Dynamic range issues nowadays resolved with dual receiver designs (& SFL)

- Canopy transmission losses cannot be accurately estimated -> interpretation of subsequent backscattering is ill-posed

- No two LiDAR datasets are comparable because of the radar theory explaining the influence of target geometry on the signal. Especially an issue in low-altitude acquisitions

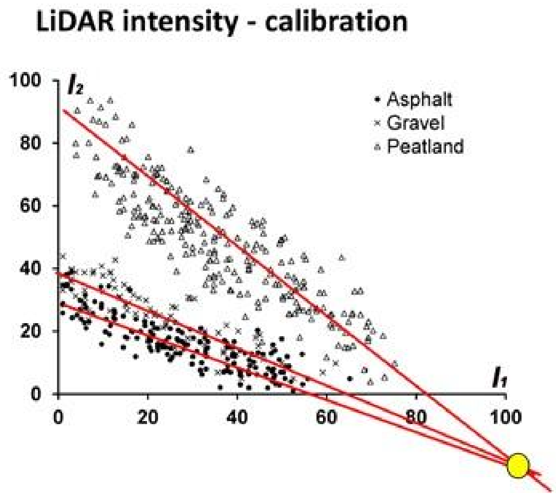

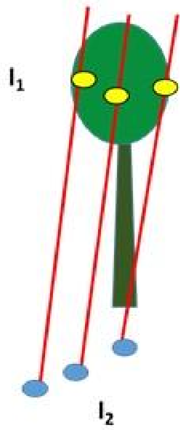

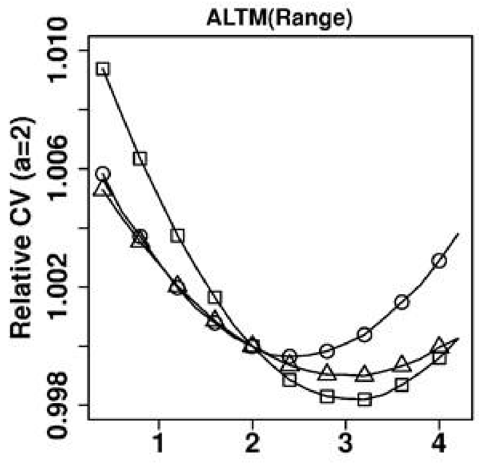

Some empirical work

Lakkasuo (62N, 24E) study in 2009, REGULAR, AFFORDABLE airborne discrete-return LiDAR from 1 km, having 1-7 pulses/m2, @ 1064 nm.

To what degree can we reconstruct hummock-hollow variation (topography) - to later predict the site type

What does LiDAR intensity data reveal about the vegetation?

Echo triggering in mire vegetation - How does the vegetation influence the geometry of near-gnd data

Area-based (10 x 10 m) habitat classification in using LiDAR features. What features are meaningful and how they describe the distinguishable characteristics of each habitat (site type)?




https://www.mv.helsinki.fi/home/korpela/Hyytiala/Ojitus_animaatio.html

Siikaneva study in 2014-15. Helicopter-borne (300 m AGL) simultaneous acquisition of waveform recording lidar (SWIR @1550 nm) and multi-view RGB-imagery. Classify (ombrotrophic pine-ridge) bog microforms at 20 cm resolution for a 16-ha area. 20-60 pulses/m2.

Can we harness the target-specific 'BRDF-effects' to enhance interpretation?

Can we reconstruct the topography accurately enough and come up with good topographic predictors of the microforms?

What is the benefit from having both the discrete-return data and waveforms, do WFs carry information about the presence and type of field layer?

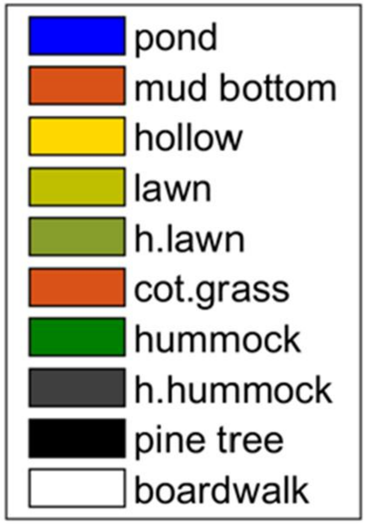

Major findings

Lakkasuo Habitat classification with LiDAR

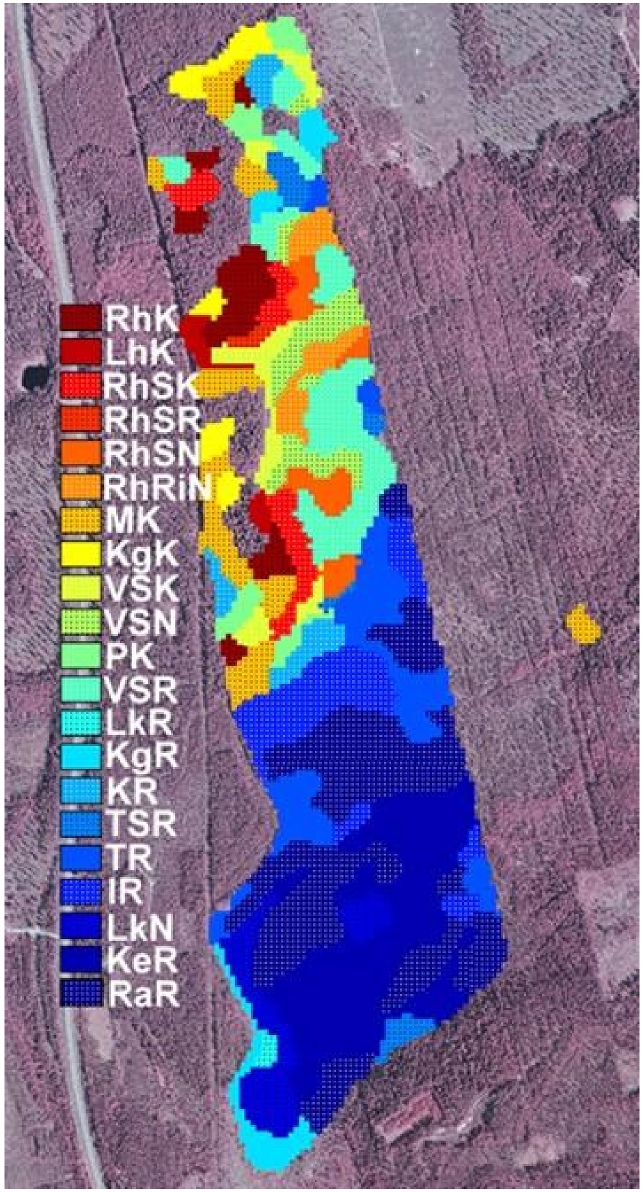

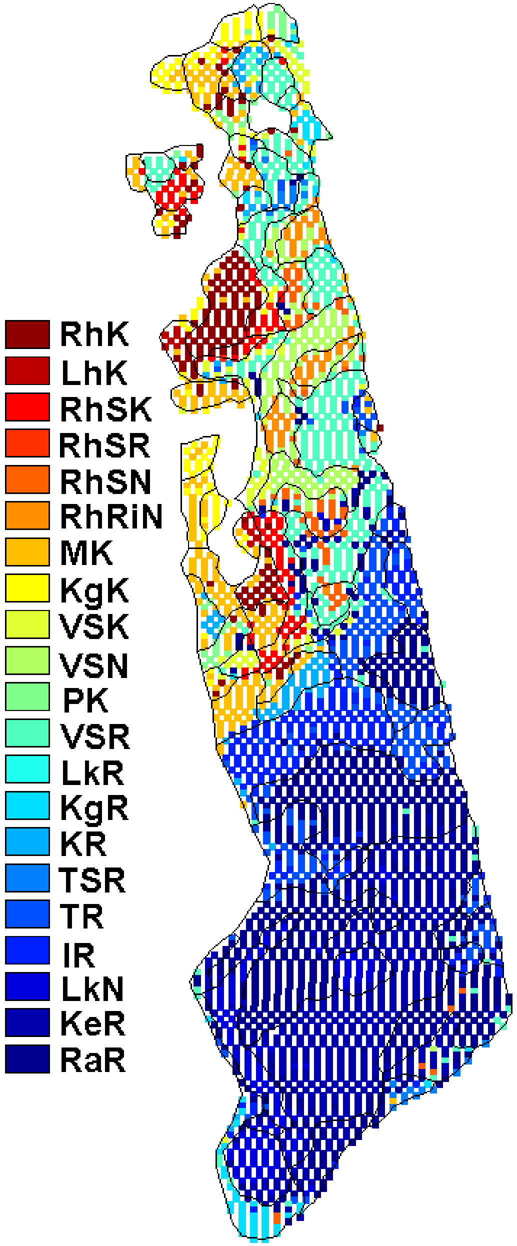

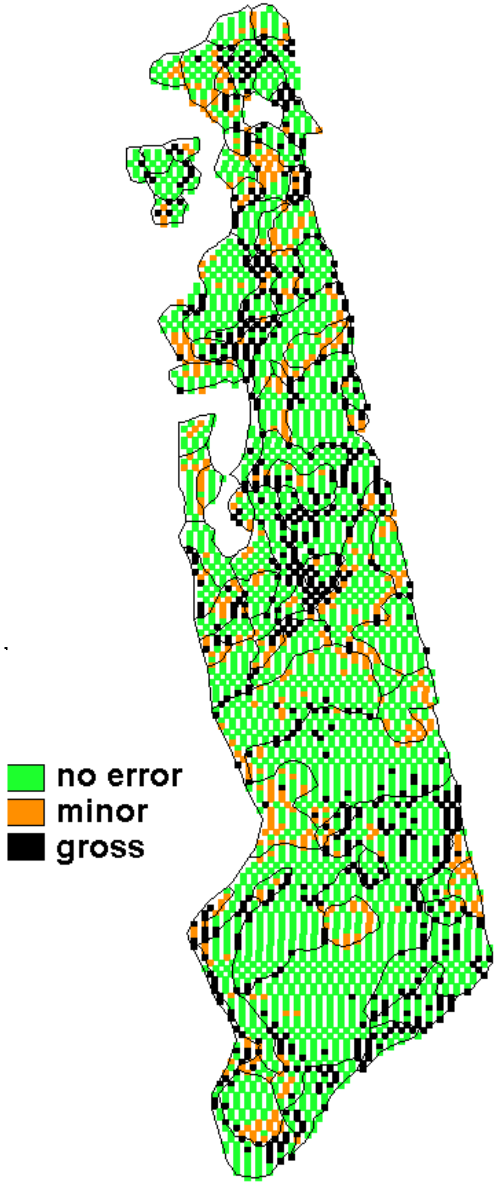

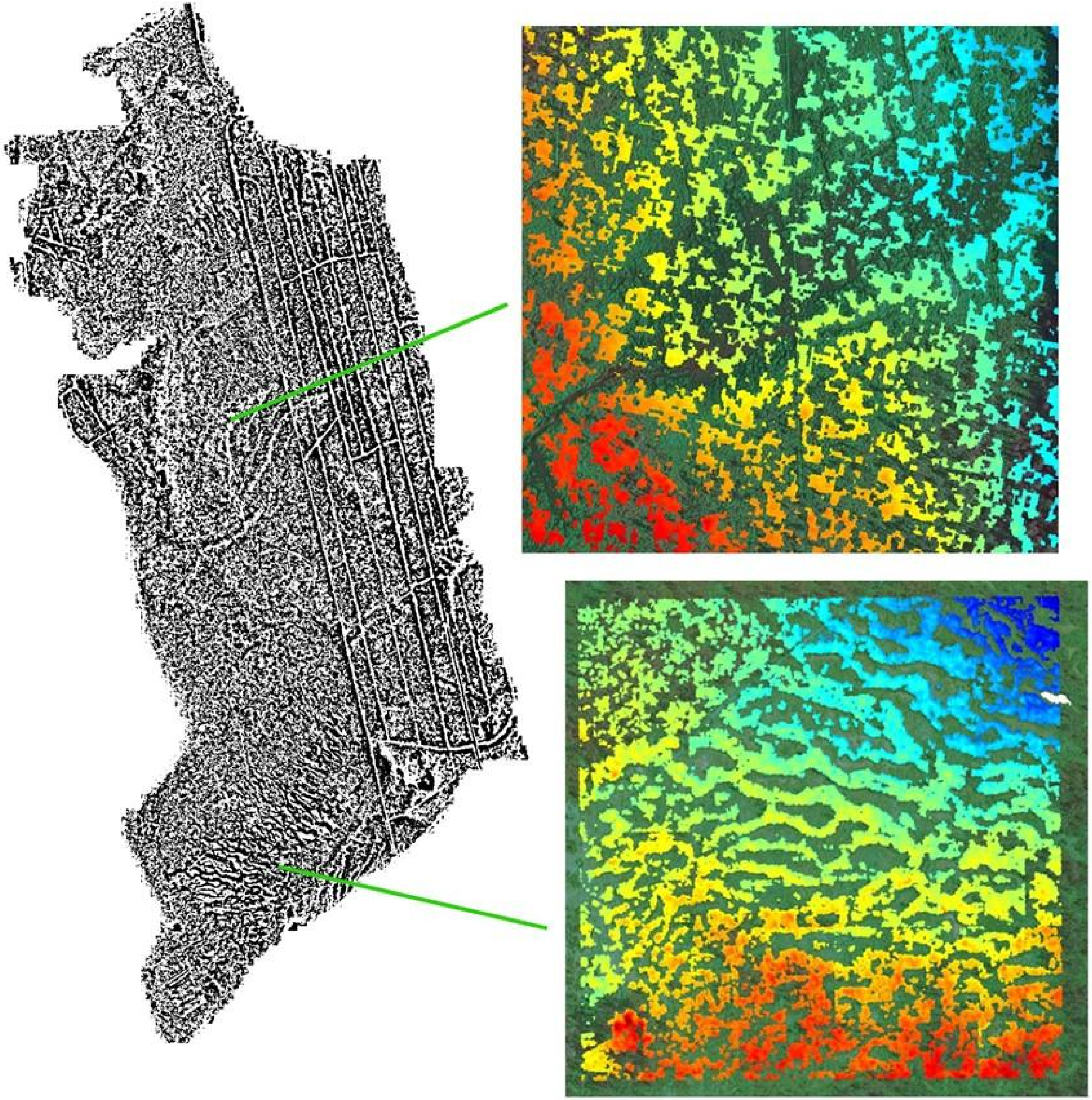

Lidar height distribution (canopy profiling) was characteristic to growing stock (site)

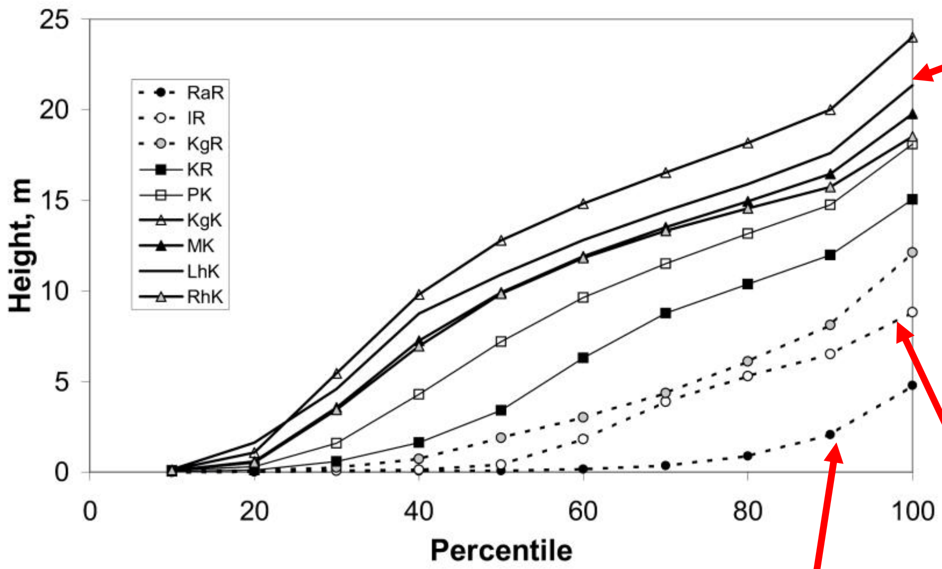

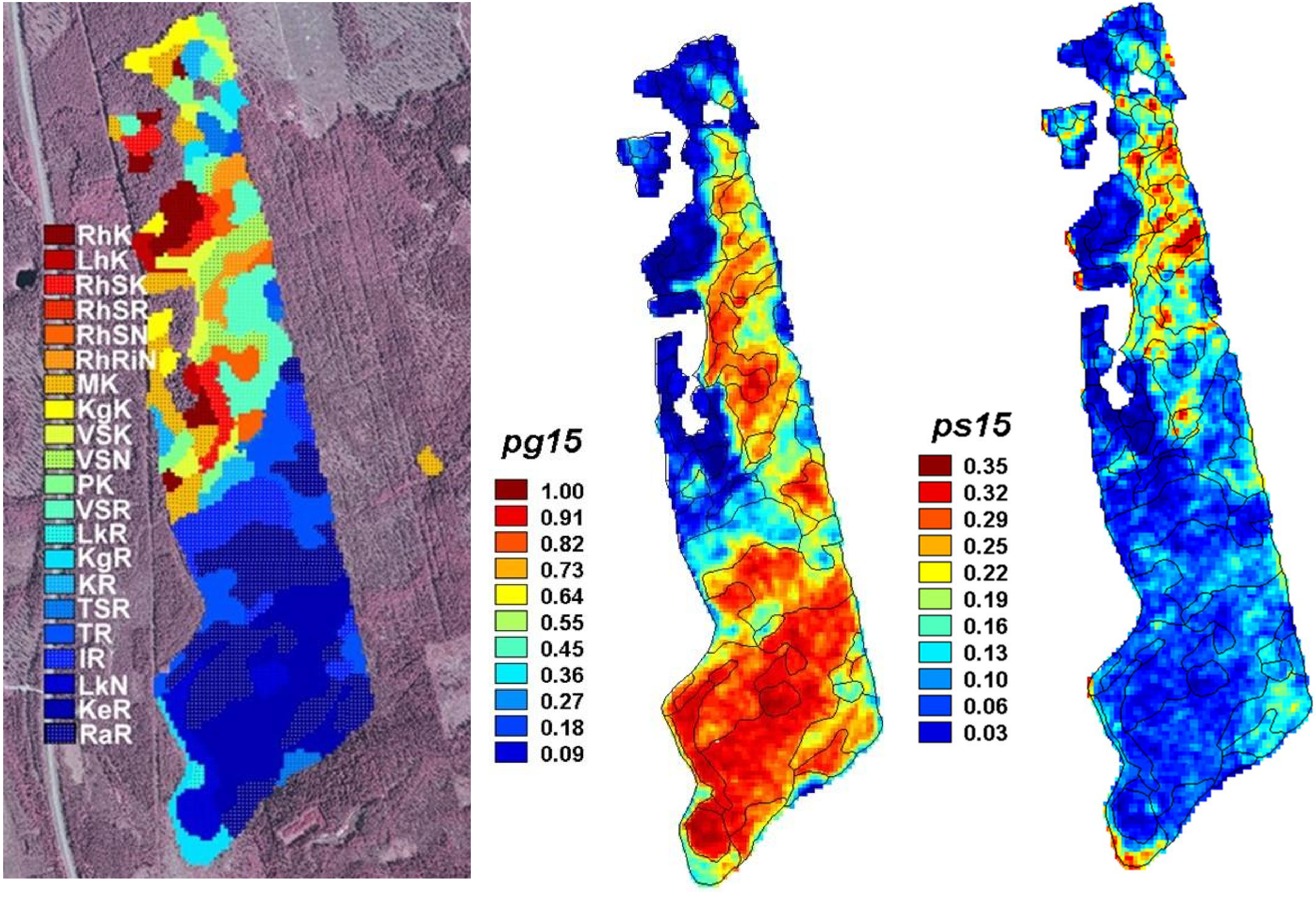

RhK
LhK
RhSK
RhSR
RhSN
RhRiN
MK
KgK
VSK
VSN
PK
VSR
LkR
KgR
KR
TSR
TR
IR
LkN
KeR
RaR
pg15
1.00
0.91
0.82
0.73
0.64
0.55
0.45
0.36
0.27
0.18
0.09
ps15
0.35
0.32
0.29
0.25
0.22
0.19
0.16
0.13
0.10
0.06
0.03

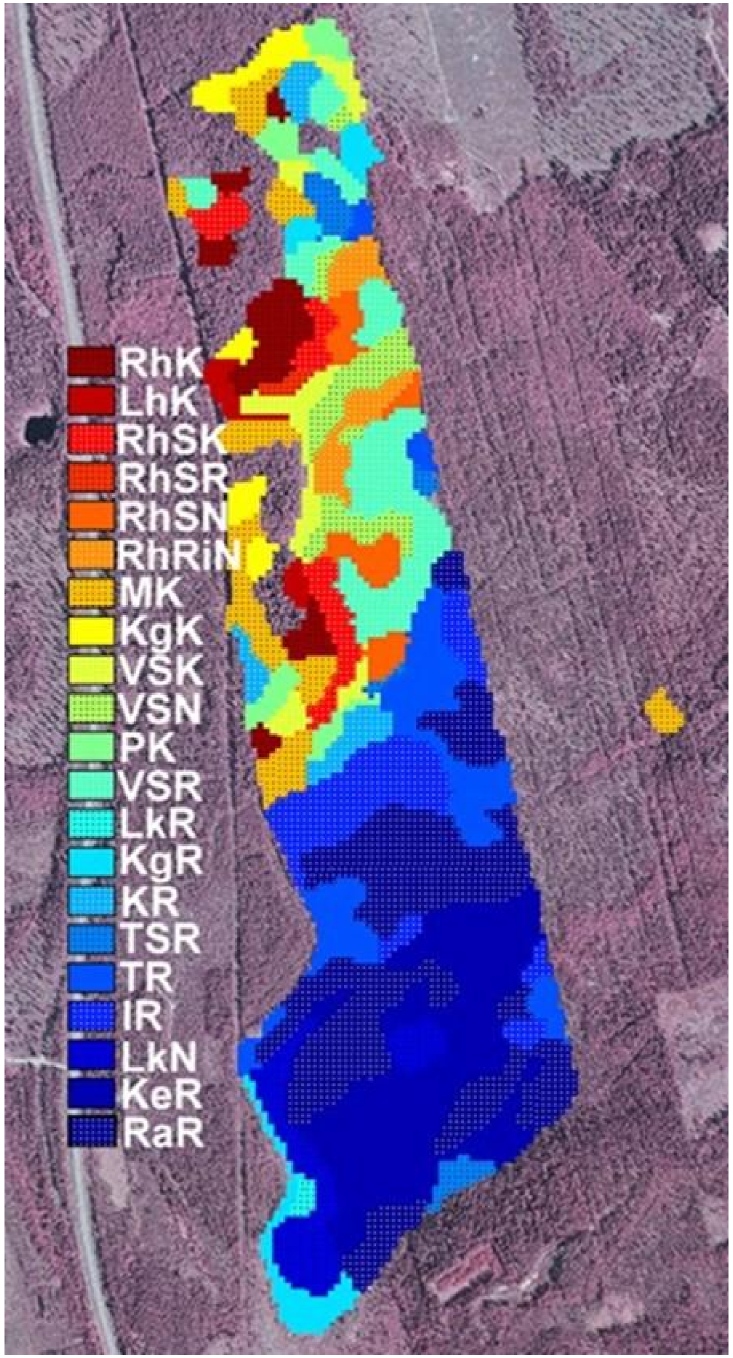
RhK
LhK
RhSK
RhSR
RhSN
RhRiN
MK
KgK
VSK
VSN
PK
VSR
LkR
KgR
KR
TSR
TR
IR
LkN
KeR
RaR

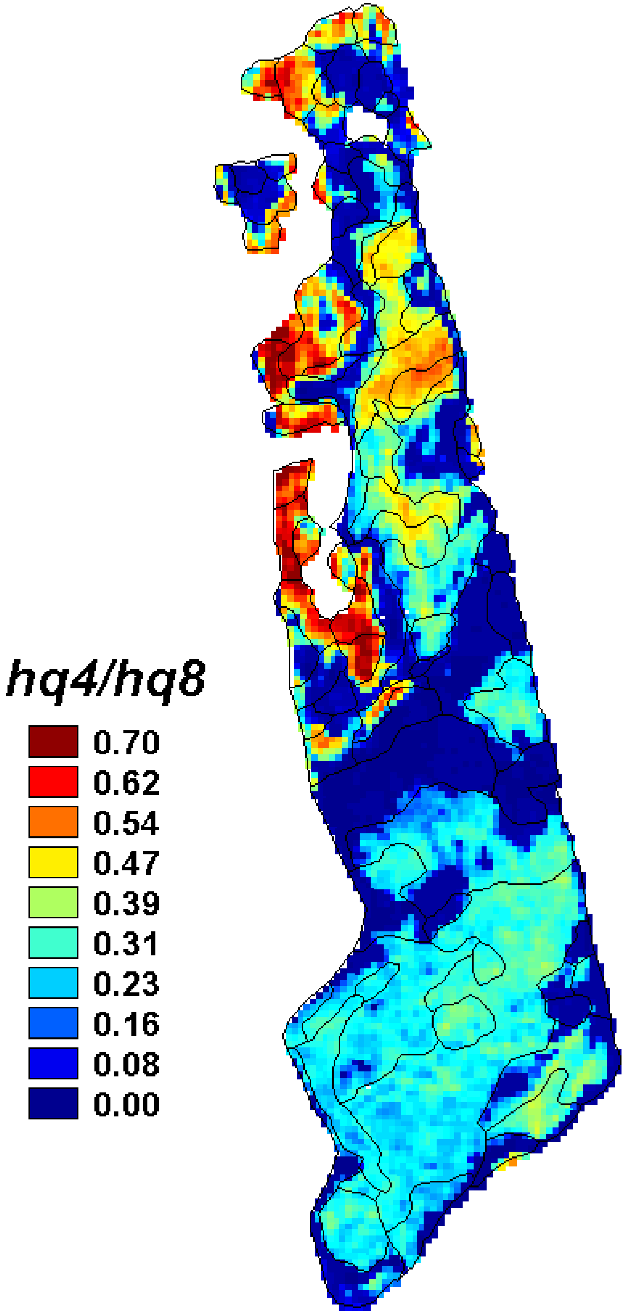
hq4/hq8
0.70
0.62
0.54
0.47
0.39
0.31
0.23
0.16
0.08
0.00

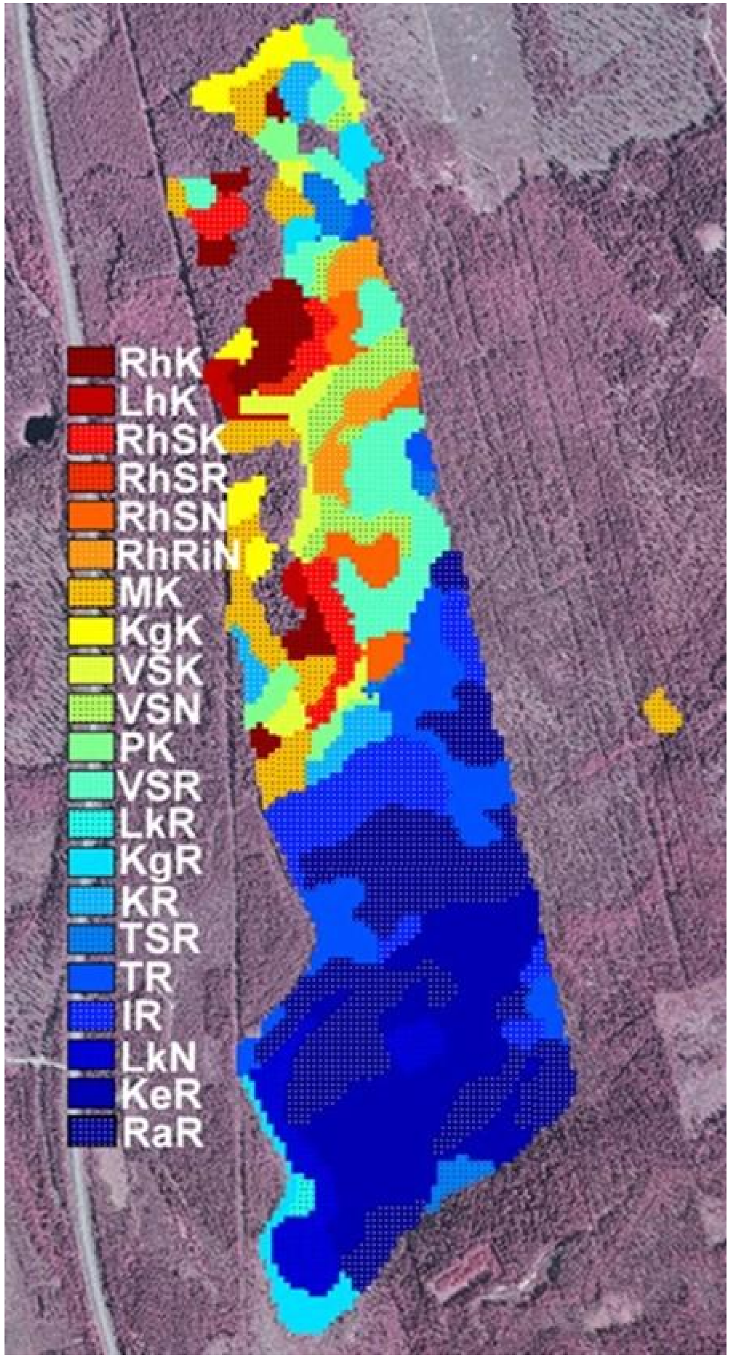
RhK
LhK
RhSK
RhSR
RhSN
RhRiN
MK
KgK
VSK
VSN
PK
VSR
LkR
KgR
KR
TSR
TR
IR
LkN
KeR
RaR

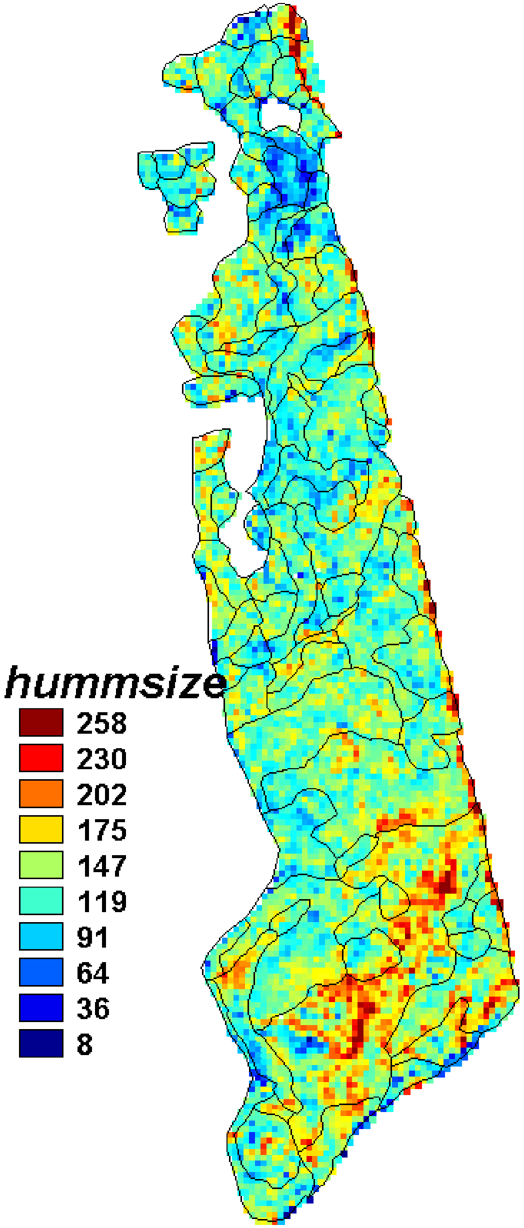
hummsize
258
230
202
175
147
119
91
64
36
8

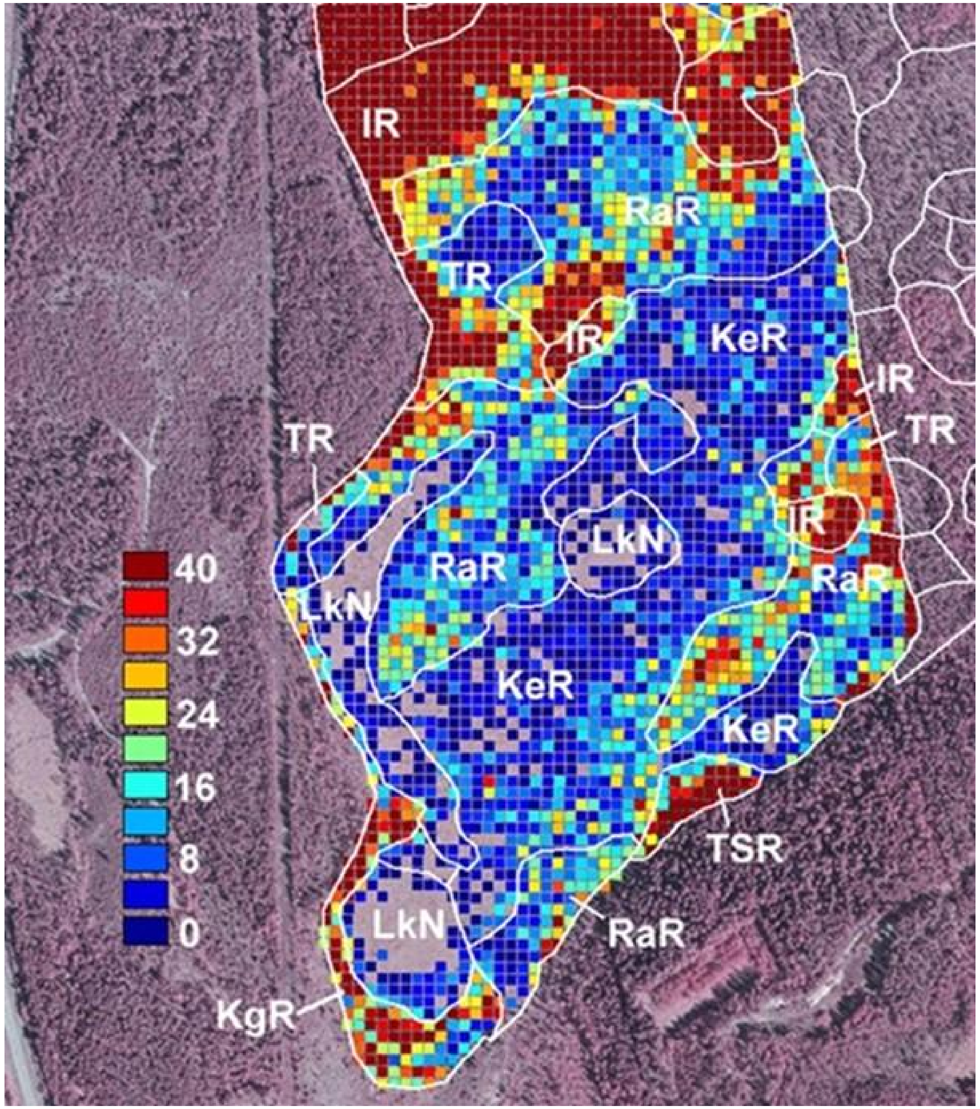

IR
RaR
TR
IR
KeR
IR
TR
TR
LkN
IR
RaR
RaR
LkN
KeR
KeR
TSR
LkN
RaR
KgR
40
32
24
16
8
0

Table 11. Confusion matrix of SVM mire site-type classification using Expert variables from 20 × 20-m squares. Classification accuracy was 50% cells denote minor errors in site-type classification. Allowing for minor errors, the accuracy was 70%.

	Genuine forested types									Composite types								Treeless mires				Classification accuracy, %	
	Spruce mires						Pine mires			Minerotrophic						Ombro		Minerotrophic			Om		
	RhK	LhK	MK	KgK	PK	KR	KgR	IR	RaR	RhSK	RhSR	VSK	VSR	LkR	TSR	TR	KeR	RhSN	RhRiN	VSN	LkN	With minor	Correct cases only
RhK	**69**		45	5		1	9			5			2									84	51
LhK	5	**6**	16	6			2			1												75	17
MK	24		**126**	17	4	1	11	4		1		4	2		2							87	64
KgK	8	1	31	**41**	2					1					1							87	48
PK	11		45	2	**10**		1	2		2		2	2									75	13
KR	1		7		2	**16**	7	4	19	1		7	23		3	4	2	2				26	16
KgR			20		2		**30**	17		2			8									62	38
IR			2					**146**	51				3		2	22						74	65
RaR								21	**452**				17		4	22	111	4	1	2	1	75	71
RhSK	17		14	1	4		6	1	8	**25**		13	16			1						36	24
RhSR	1		3							5	**0**		1									10	0
VSK	2		11		5		7	1	7	8		**16**	38			2	1			1		24	16
VSR	1				3		5	5	65	4		6	**148**		4	6	6	3	1	7		58	58
LkR								2	5					**0**	1		3					45	0
TSR			5		1		1	1	13	1		5	17		**12**	1						53	23
TR			8			1		56	111			5	16		2	**66**	9			2		85	24
KeR								1	125						6		**375**	1			1	74	74
RhSN									13			4	22				14	**10**		26		40	11
RhRiN									7			6	8				1	7	**31**	25		74	36
VSN			3		1			2	13			1	16		1		3	13	9	**67**		69	52
LkN									11							1	112			1	**24**	92	16

SIIKANEVA microforms with WF-LiDAR and multi-view RGB

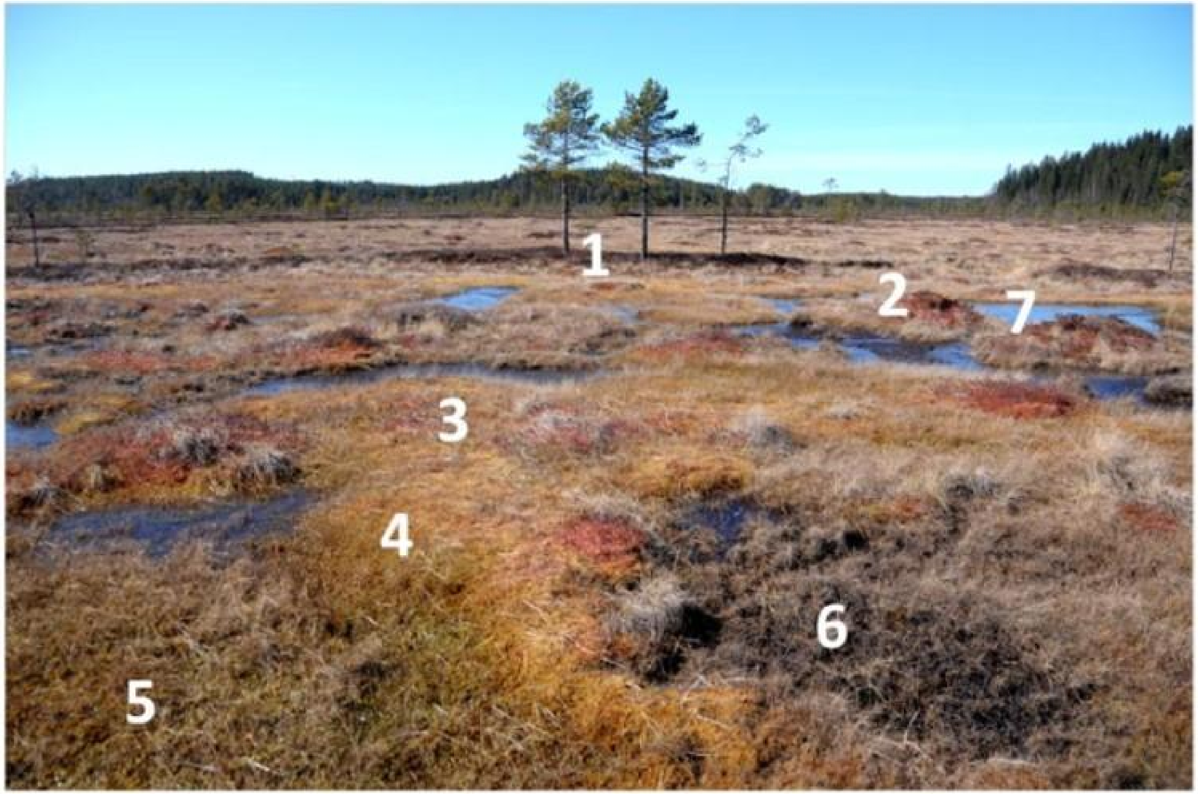

FIG 1 A close range view of the study area with outlined vegetation classes: 1 = high hummock (HHU) ridge with 1–6-m high pine trees, 2 = hummock (HU), 3 = high lawn (HL) with reddish *Sphagnum rubellum*, 4 = Lawn (L), 5 = hollow (HO), 6 = mud-bottom (MB) with *Rhynchospora alba*, and 7 = water (W). Cottongrass (GC) tussocks are pale greyish.

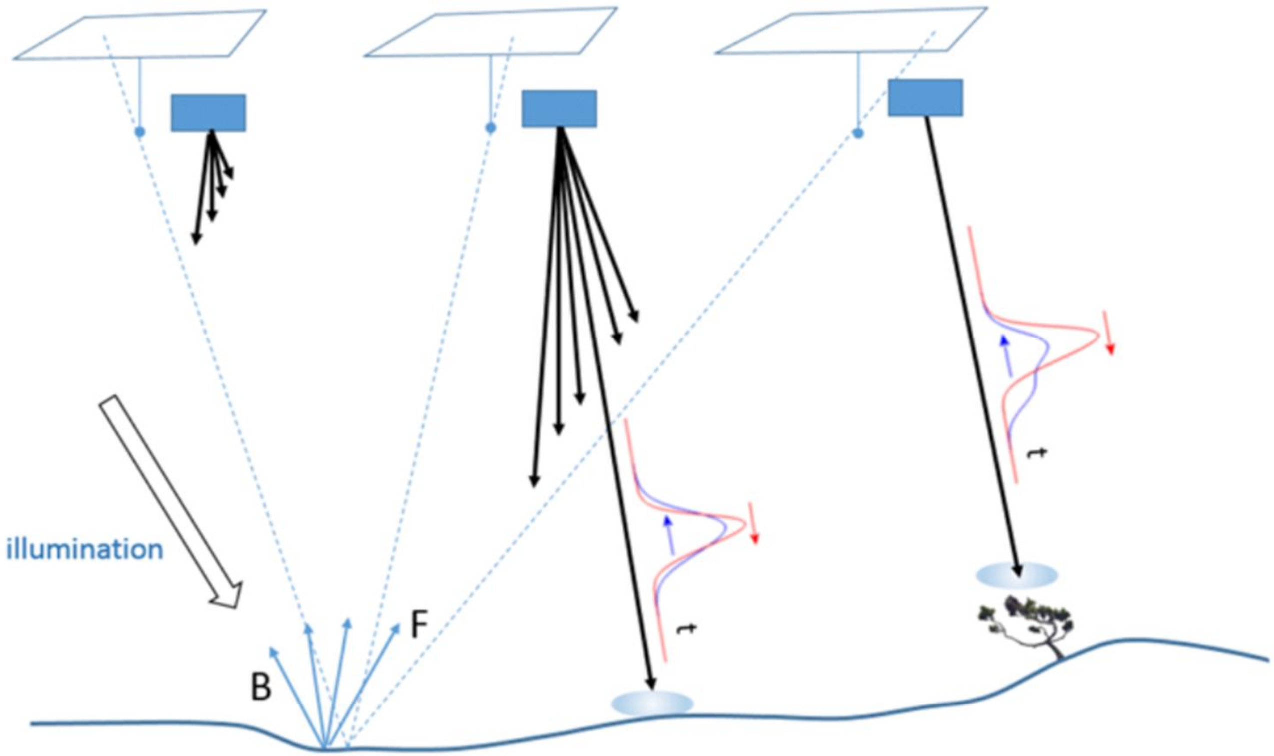

Fig. 2. Illustration of 'sensor fusion on the bog surface'. Camera and LiDAR are operated concurrently such that the same surface patch is seen in several images (exposed at short intervals) and is sampled densely by LiDAR. The return waveform (blue) preserves its shape in well-defined surfaces, while a tilted or rough surface, or, volumetric vegetation extends it. Image observations are influenced by directional reflectance properties of the targets, as the view direction (camera-target ray) changes, when the camera is moved. B = backscattering, F = forward-scattering.

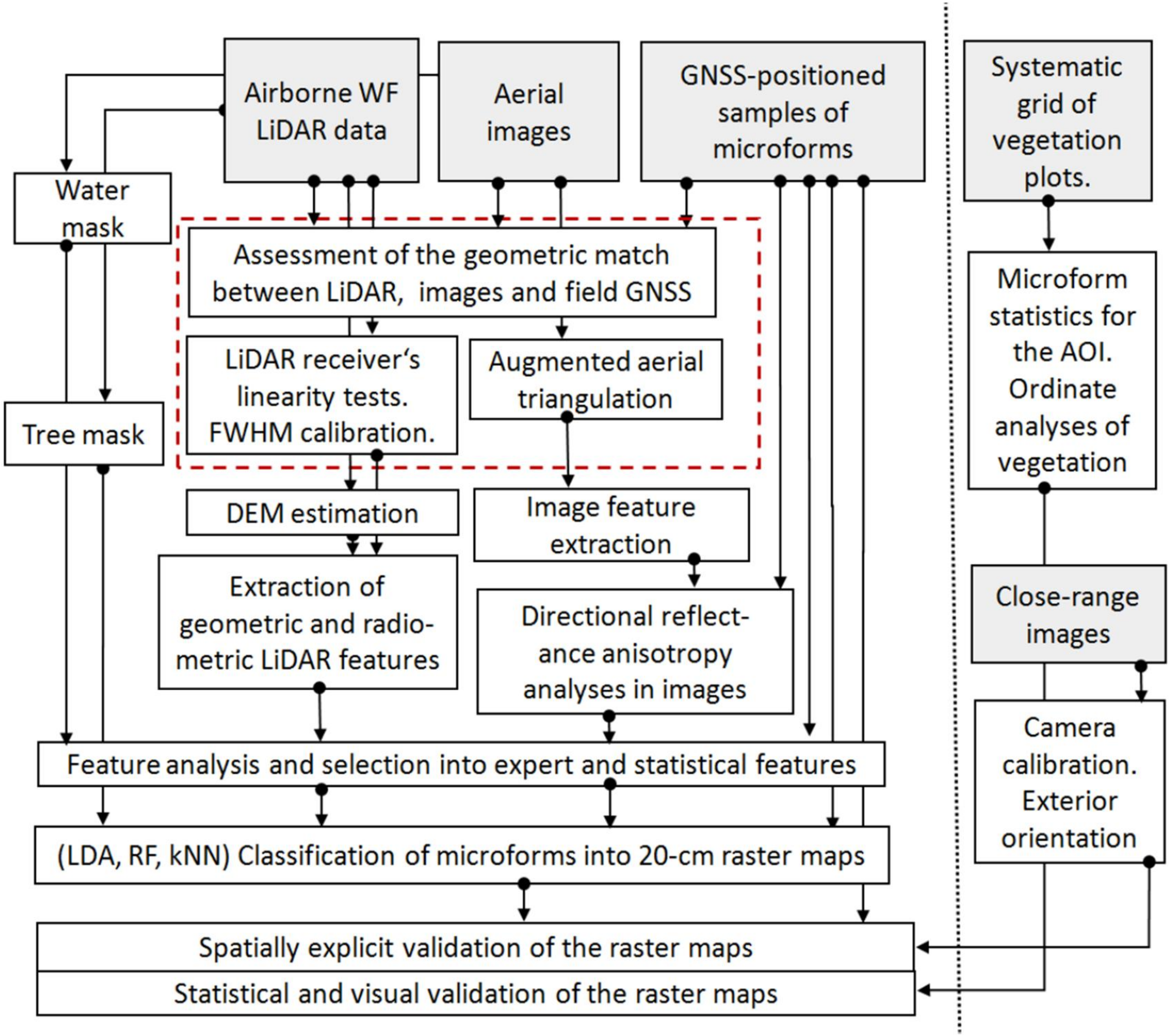
Airborne WF LiDAR data
Aerial images
GNSS-positioned samples of microforms
Systematic grid of vegetation plots.
Water mask
Assessment of the geometric match between LiDAR, images and field GNSS
LiDAR receiver's linearity tests. FWHM calibration.
Augmented aerial triangulation
Microform statistics for the AOI. Ordinate analyses of vegetation
Tree mask
DEM estimation
Image feature extraction
Close-range images
Extraction of geometric and radio-metric LiDAR features
Directional reflect-ance anisotropy analyses in images
Camera calibration. Exterior orientation
Feature analysis and selection into expert and statistical features
(LDA, RF, kNN) Classification of microforms into 20-cm raster maps
Spatially explicit validation of the raster maps
Statistical and visual validation of the raster maps

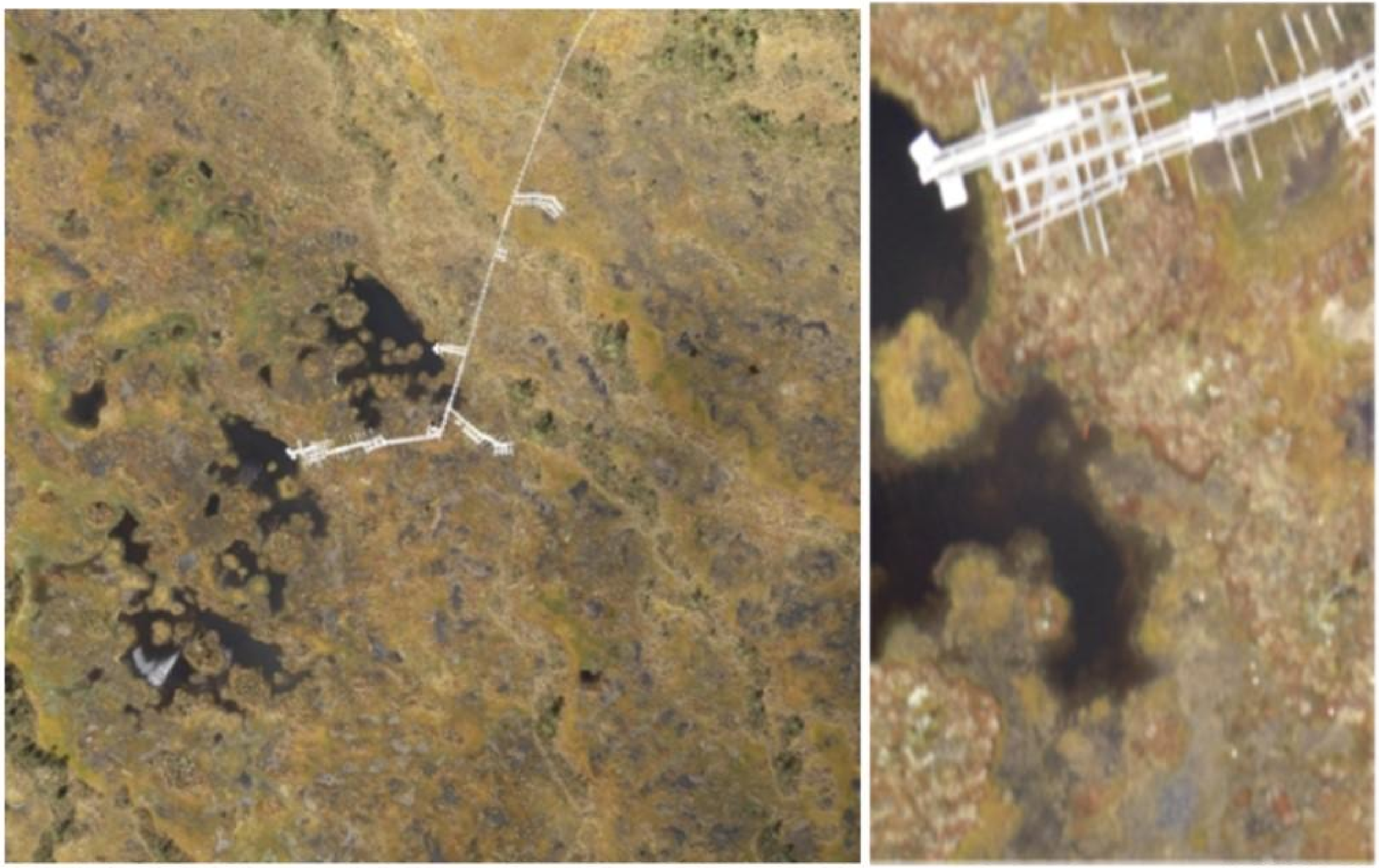

FIG 4 A 200×200-m aerial image from May 2013. The EC tower is in the center (350999.7E, 6859303.5N in UTM35). Darkest surfaces are water (W). Grayish surfaces are mud-bottoms (MB). Shadows of 1−5-m-high pines are barely visible on the ridge hummocks. Green-yellowish depicts hollow (HO) and lawn (L) surfaces (Table 1). The sub-image on the right shows an area of 19 by 28 meters.

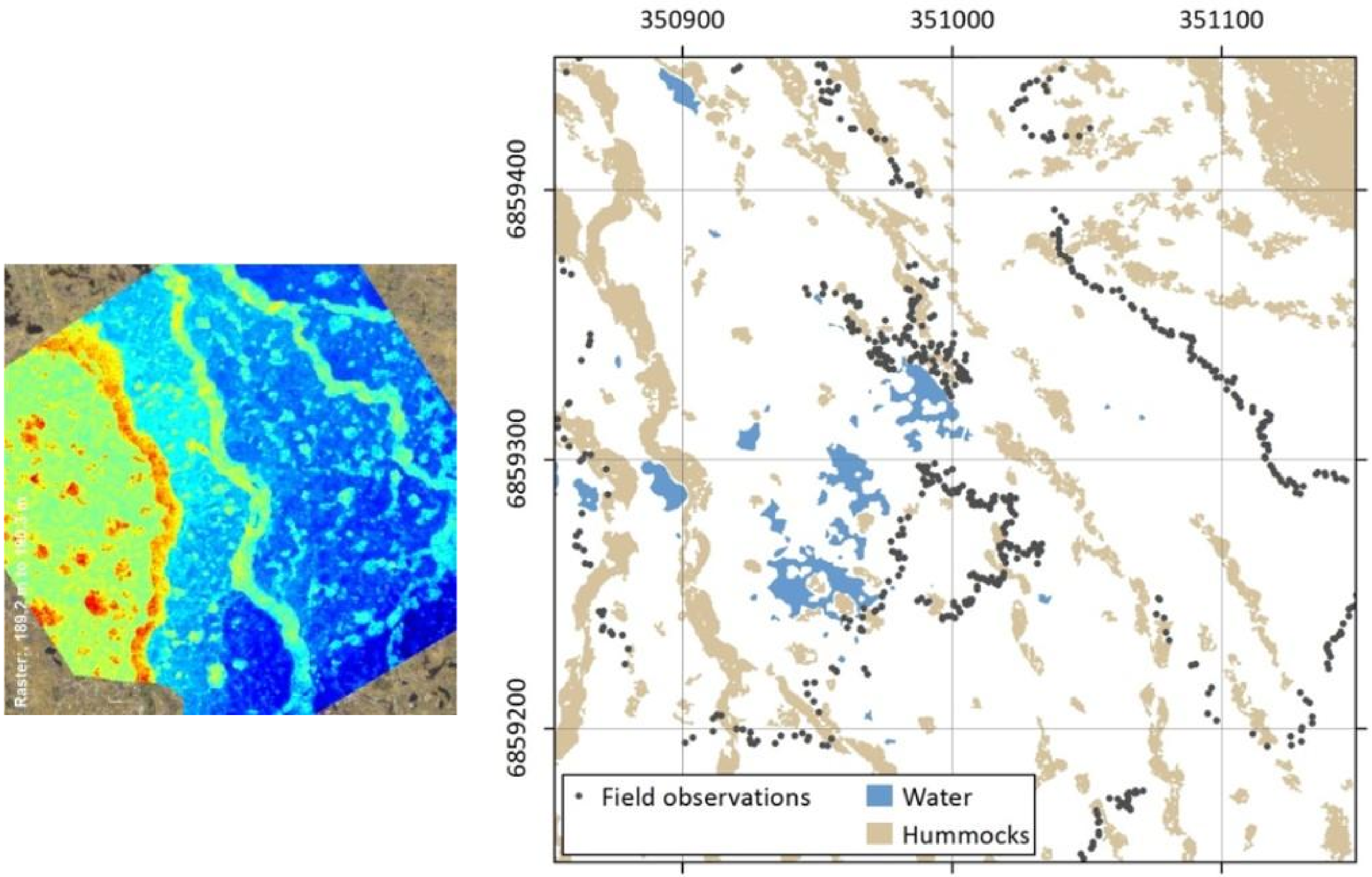

FIG 5 Location of the 756 vegetation field plots of 2014.

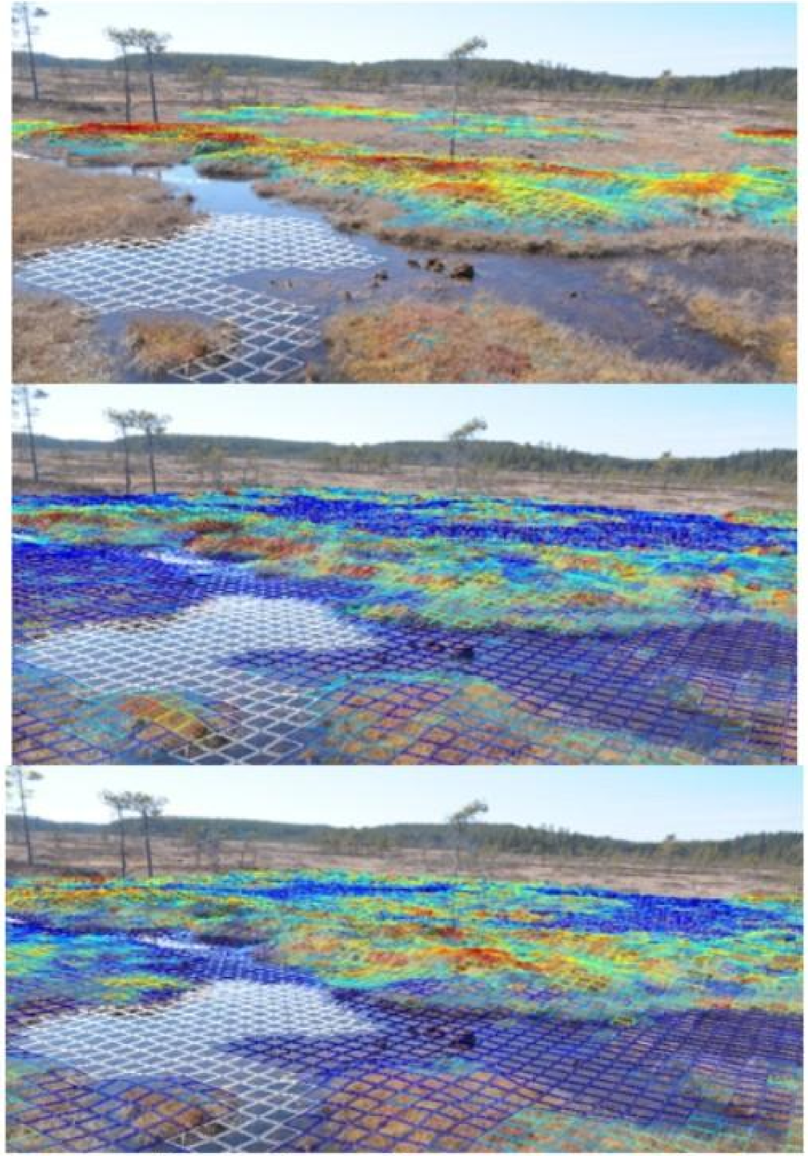

FIG 6 Illustration of the HU-IND (large values only), FLATNESS and INTENSITY feature maps. The white cells are WATER. FLATNESS peaks in slopes. INTENSITY is high in hummocks and low in water, hollow and mud-bottom.

TABLE 4 DEM features implemented in QGIS (Quantum GIS Development Team 2015), ArcGIS (Esri Ltd, Redlands, CA, USA), GRASS GIS (GRASS Development Team 2015), or in an in-house photogrammetric workstation.

Feature	Description
SDEV	Standard deviation in a 3×3 (30×30-cm) window. Local surface roughness and/or slope.
SLOPE & SRANGE	QGIS 2.10: maximum rate of change in a 3×3 window. The range of slope values.
HU-IND	A ‘hummock index’ that looks for the minimum elevation up to a distance, in eight cardinal directions, and computes the difference.
DEPR-IND	A ‘depression index’. Collects elevations from the eight cardinal directions up to a distance and fits univariate regression to each direction. Computes the sum of the coefficients, which are assigned +1 or −1 for positive or negative coefficients. A ‘perfect peak’ is 8, while −8 corresponds to a depression. Finds the small-scale variation in the mire surface.
FLATNESS	Computed in a window by taking the smallest sum of elevation differences among the eight cardinal directions. Indicates if the point of interest has a local flat surrounding in at least one of the directions.
DISTHUM	Distance to closest hummock border (HU-IND > 0.2 m). The thresholded HU-IND raster was processed twice with the majority filter in the Spatial Analyst of ArcGIS. Then, unique labels were given for each contiguous area. This raster was converted into vector format and areas smaller than 10 m^2 were removed. Finally, the Euclidean distance tool was applied to create a map with distances to the closest hummock.
Texture features	Textural features Contrast, Entropy, Angular Second Moment and Inverse Distance Measure were derived in GRASS. The features were computed in 3×3 and 5×5 neighborhoods.

Table 6. Partition of DN (mean values in 5x5 window) variance between the terms of the mixed-effects models (Eq. 3). Percentages (%) of total variance.

	Anisotropy			Target			Residual		
Class	R	G	B	R	G	B	R	G	B
HHU	31	28	34	60	62	56	9	10	10
HU	20	13	17	61	75	69	19	12	14
HL	12	7	10	69	83	77	19	10	12
L	7	8	8	79	82	80	14	10	12
HO	5	12	8	83	73	81	12	15	11
MB	5	5	4	79	74	79	16	21	17
CG	25	17	25	67	74	68	8	9	7

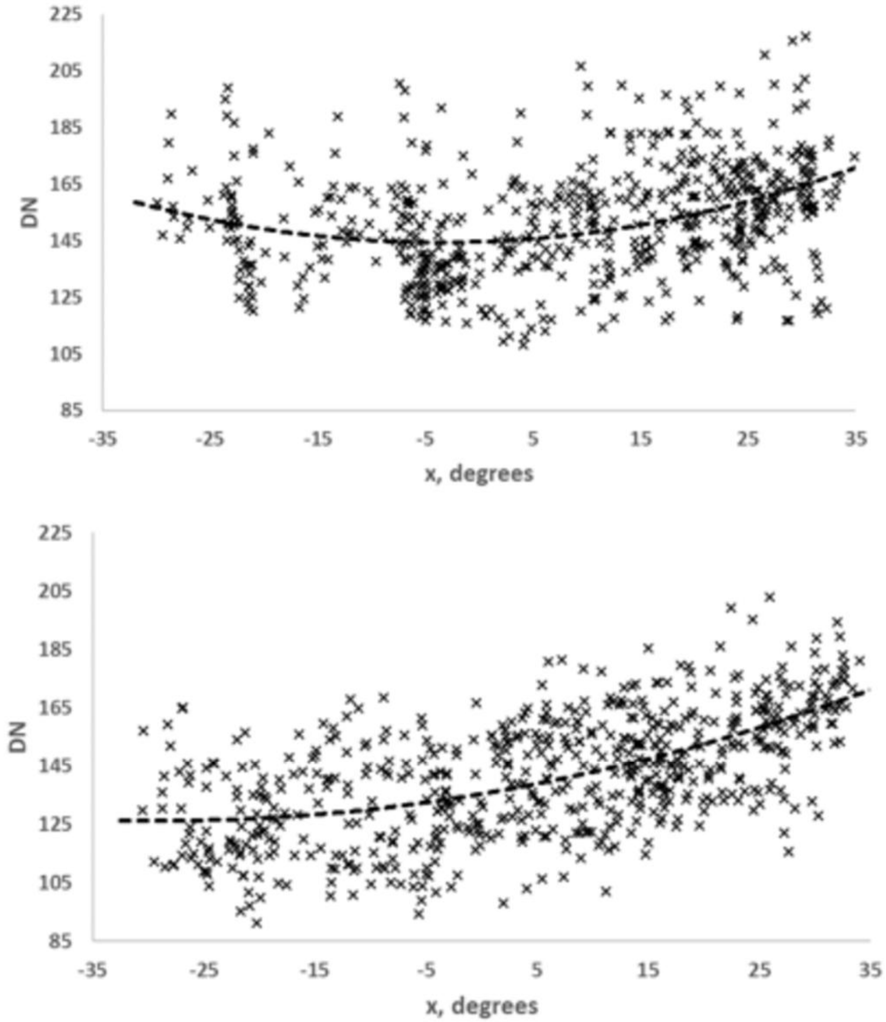

FIG 8 GRN band mean feature as a function of x in Eq. 1. HO shows an increase also in the forward scattering geometry (x<0°), while HHU shows a decrease.

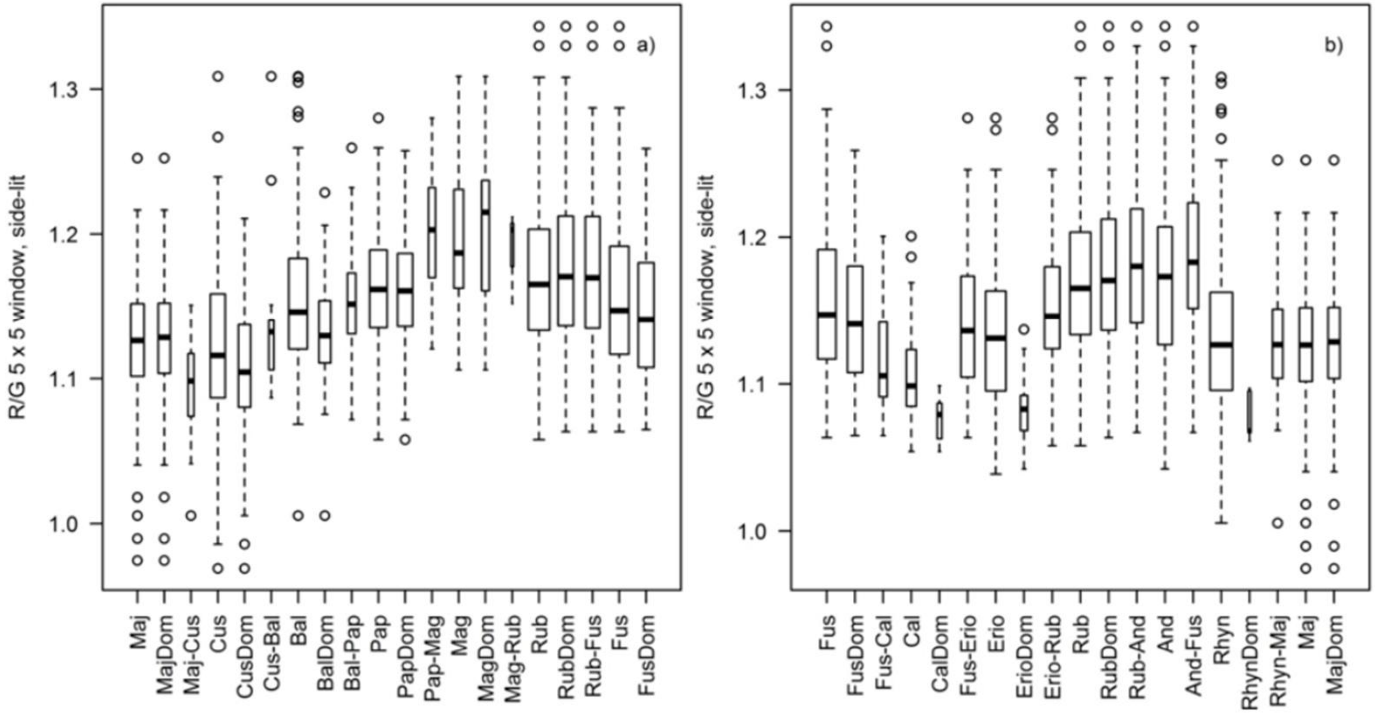

FIG 10 Boxplot comparison of the R/G image feature in plots vegetated by (a) *Sphagnum* mosses only and (b) *Sphagnum* mosses with field layer vegetation. The labels 'XXX', 'XXXDom', 'XXX-YYY' are interpreted as 'Species XXX is found', 'Species XXX dominates' and 'Both XXX and YYY are found', respectively. Abbreviations are given in Table 2. Azimuth difference is limited to 90°±45° (stratum) to constrain the directional effects. Note that groups are not limited and for example *S. balticum* can occur in groups 'Maj', 'MajDom', 'Maj-Cus', etc.

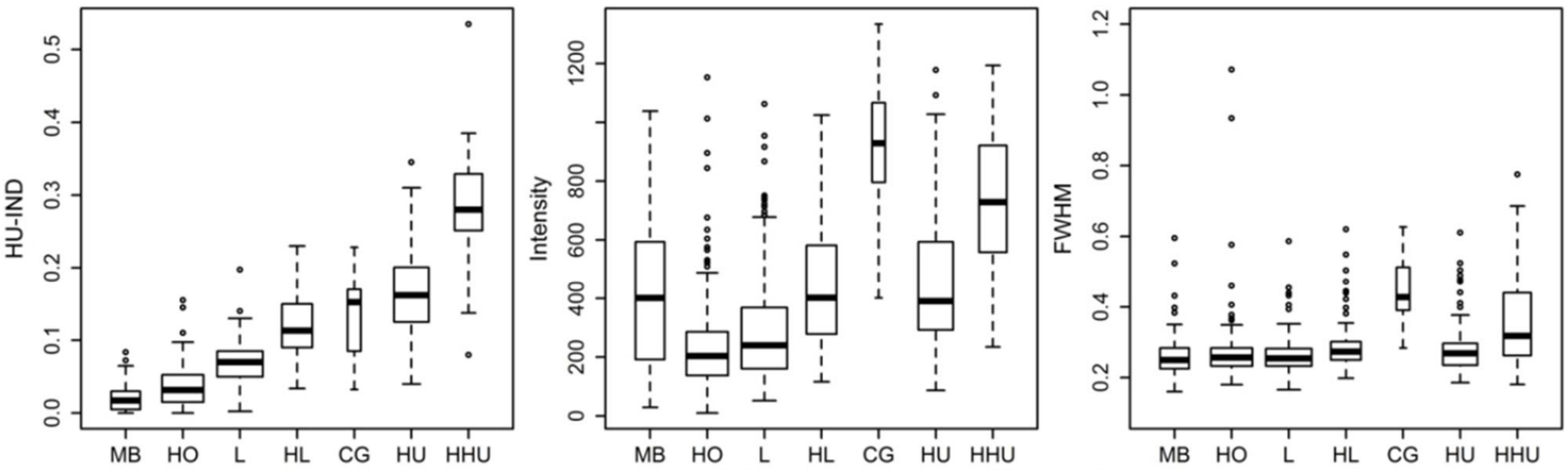

FIG 12 Boxplot graphs of three LiDAR features. FWHM refers to ECHOW feature.

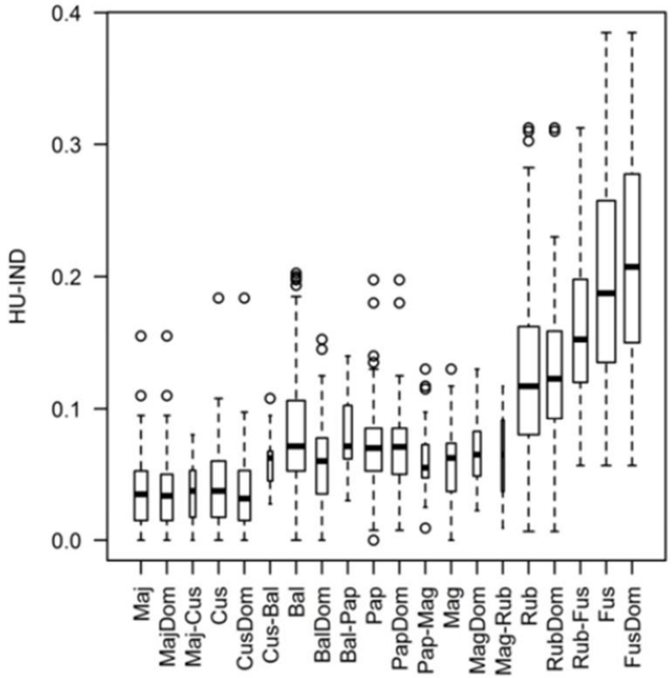

FIG 13 Boxplot of the hummock index (HU-IND) in vegetation plots, where *Sphagnum* moss species occurred in various combinations. See also Figure 11 for an interpretation of the classes.

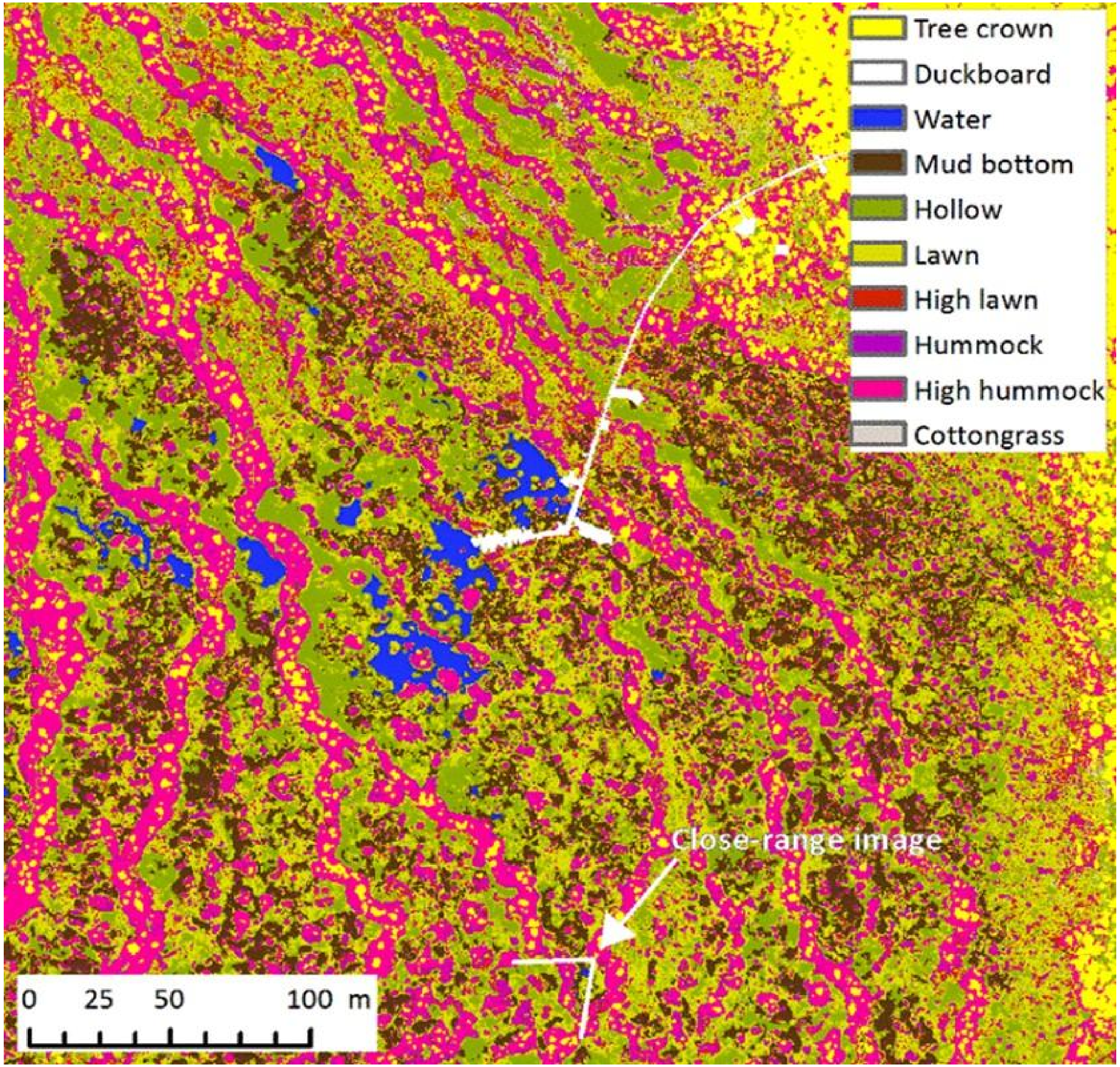
Tree crown
Duckboard
Water
Mud bottom
Hollow
Lawn
High lawn
Hummock
High hummock
Cottongrass
Close-range image
0 25 50 100 m

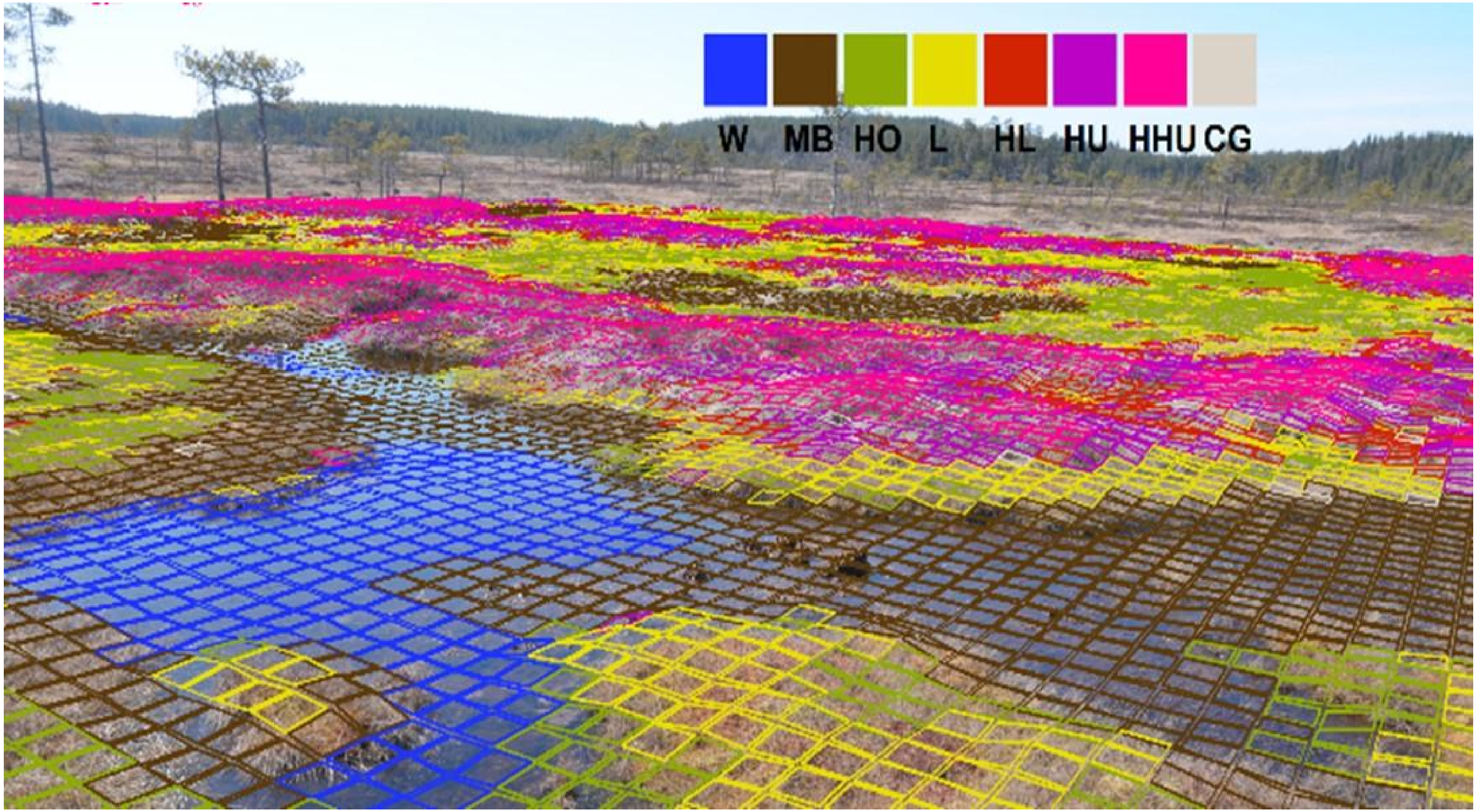
W MB HO L HL HU HHU CG

TABLE 11 Comparison of classification results (%) within a radius of 150 m from the EC tower. The standard error estimates in percentage points are given in parentheses for the 2012 (systematic cluster-based) field inventory and are based on the random sampling assumption.

Class	RF	LDA	Field
W	2.3	2.3	2.0 (0.9)
MB	15.9	17.2	15.8 (2.0)
HO	19.9	14.2	19.2 (2.4)
L	26.9	29.5	18.2 (2.2)
HL	7.2	5.0	12.8 (1.8)
CG	0.6	5.3	- (-)
HU	11.0	10.9	10.8 (1.6)
HHU	16.2	15.6	21.2 (2.5)

Table 12 Neighborhood relations between classes (%). For example, 36.7% of the 3×3-neighborhood pixels of high lawn (HL) pixels belong to the same class, while 23% belong to hummock (HU). DB = white wooden duckboard (manually delineated). (See Figure 14). All cells are non-zero.

	MB	HO	L	HL	CG	HU	HHU	Tree	W	DB
MB	<u>82.5</u>	5.4	8.6	1.3	0.1	1.4	0.3	0.1	0.3	0.0
HO	3.9	<u>71.9</u>	21.7	0.8	0.2	0.4	0.5	0.5	0.1	0.0
L	4.3	15.2	<u>66.3</u>	7.9	0.9	4.4	0.7	0.3	0.0	0.0
HL	2.5	2.2	30.0	<u>36.7</u>	2.0	23.0	3.1	0.4	0.0	0.1
CG	2.1	5.6	30.0	18.4	<u>27.3</u>	13.6	2.1	0.9	0.0	0.1
HU	1.8	0.7	11.5	15.7	1.0	<u>54.8</u>	14.0	0.5	0.0	0.0
HHU	0.3	0.7	1.3	1.5	0.1	10.0	<u>81.6</u>	4.5	0.0	0.0
Tree	0.1	0.7	0.5	0.2	0.0	0.4	4.7	<u>93.4</u>	0.0	0.0
W	3.3	1.6	0.9	0.1	0.0	0.1	0.1	0.0	<u>93.8</u>	0.1
DB	1.0	1.4	2.4	1.1	0.1	0.8	0.8	1.6	0.3	<u>90.5</u>

END